Systems/Circuits

Exploring Neural Dynamics in the Auditory Telencephalon of Crows Using Functional Ultrasound Imaging

Diana A. Liao,* **Eva Schwarzbach,*** and ⬤**Andreas Nieder**

Animal Physiology, Institute of Neurobiology, University of Tuebingen, Tuebingen 72076, Germany

Crows, renowned for advanced cognitive abilities and vocal communication, rely on intricate auditory systems. While the neuroanatomy of corvid auditory pathways is partially explored, the underlying neurophysiological mechanisms are largely unknown. This study used functional ultrasound imaging (fUSi) to investigate sound-induced cerebral blood volume (CBV) changes in the Field L complex of the auditory telencephalon in two female crows. fUSi revealed frequency-specific CBV responses, showing a tonotopic organization within the Field L complex, with low frequencies in the posterior dorsal region and high frequencies in the anterior ventral region. Machine learning analyses showed fUSi signals could be used to classify sound types accurately, in both awake and anesthetized states. Variable CBV responses to longer sound stimuli suggest a delineation of subregions within the Field L complex. Together, these findings highlight the potential of fUSi for providing high-resolution insights into functional systems in corvids, enabling future exploration of experimental task-related cognitive dynamics.

Key words: auditory; corvid songbird; crow; Field L complex; functional ultrasound imaging; tonotopy

---

Significance Statement

This study highlights the use of functional ultrasound imaging (fUSi) to explore auditory processing in crows, marking the first application of this technique in songbirds. By revealing the frequency map of the crow's auditory system and demonstrating the ability of fUSi to classify sound types, the research uncovers the neural dynamics supporting complex auditory functions. The findings suggest conserved auditory organization across avian species and provide insights into the evolution of audiovocal behaviors in birds. This work paves the way for future studies on the neural underpinnings of cognition and communication in corvids, offering significant implications for comparative neuroscience and neuroethology.

Introduction

Corvids—crows, ravens, and jays—are the largest members of the songbirds and are known for their exceptional cognitive abilities (Emery and Clayton, 2004; Taylor, 2014; Nieder, 2023). They utilize their behavioral flexibility to engage in intricate audiovocal communication. Corvids possess an impressive ability to produce a diverse range of sounds, including the imitation of human speech sounds (Coombs, 1960; Brown, 1985; Bluff et al., 2010). They strategically use their vocalizations to navigate complex social dynamics, signaling identity, familiarity, dominance, and

group membership, thus demonstrating sophisticated acoustic social recognition (Hopp et al., 2001; Kondo et al., 2010; Wascher et al., 2012; Mates et al., 2015; Szipl et al., 2017; Cunha and Griesser, 2021; Martin et al., 2024). In particular, crows exhibit elaborate cognitive control over their vocalizations, a skill supported by precise audiovocal feedback mechanisms (Brecht et al., 2019; 2023; Liao et al., 2024; 2025). These remarkable traits are underpinned by the corvids' advanced auditory processing capabilities.

The corvids' auditory system, known in birds as the Field L complex—analogous to the mammalian auditory cortex—plays a key role in processing and interpreting sounds. Recent research has begun to uncover the neuroanatomy of the telencephalic audiovocal pathways in crows (Kersten et al., 2021; 2022; 2024; Moll et al., 2024), but the neurophysiological mechanisms remain unexplored. Additionally, communicative behaviors emerge from dynamic interactions of distributed brain areas such as those for vocal perception (e.g., the Field L complex) and those for vocal production (e.g., the song system; Mooney, 2009). Thus, a neuroimaging method with a large field of view is critical to help uncover the substrates for vocal communication. Here, we aim to investigate the auditory telencephalon of

crows using neuroimaging, specifically functional ultrasound imaging (fUSi), an emerging technique not yet applied to songbirds.

Neuroimaging in humans primarily relies on functional magnetic resonance imaging (fMRI). fMRI is able to noninvasively capture high-resolution, real-time, and brain-wide activity by measuring changes in blood oxygenation. In recent years, fMRI has also been successfully applied to birds, including finches (Van Ruijssevelt et al., 2013; 2018), pigeons (Behroozi et al., 2020; Arya et al., 2023; Ungurean et al., 2023), and chickens (Behroozi et al., 2024). However, the technical complexity, spatiotemporal resolution, and the need for subjects to remain completely still during measurements still pose significant challenges for neuroimaging in behaving birds and other small animals. To date, fMRI in awake birds performing controlled, complex tasks necessary to study cognitive functions or vocal production remains extremely difficult to achieve.

fUSi is an emerging neuroimaging technique that overcomes some limitations of fMRI to measure brain activity through detailed images of blood volume dynamics (Mace et al., 2011, Urban et al., 2015). Offering high spatial resolution (~100 μm) and temporal resolution in the hundreds of milliseconds, fUSi uses lightweight probes to map brain activity by emitting and recording sound waves that reflect off moving red blood cells. The small, head-mounted probes make it especially well suited for use in awake, behaving animals during behavioral tasks (Sieu et al., 2015, Urban et al., 2015, Tiran et al., 2017, Takahashi et al., bioRxiv, El Hady et al., 2024). Since fUSi does not rely on magnetic fields, unlike fMRI, it could be more easily combined with other neurophysiological methods, like electrophysiology (Nunez-Elizalde et al., 2022, Claron et al., 2023), calcium imaging (Aydin et al., 2020), pharmacological manipulations (Di Ianni et al., 2024), or optogenetics (Edelman et al., 2021).

To date, fUSi has been employed in only one bird species, the pigeon (Rau et al., 2018). This proof-of-concept study demonstrated that fUSi enables the investigation of brain responses to both visual and auditory stimulation. In the current study, we leveraged fUSi to assess its suitability and sensitivity in a corvid songbird, the carrion crow (*Corvus corone*). Specifically, we explored responses to different acoustic stimuli in the corvid Field L complex, a key auditory thalamorecipient input and telencephalic processing region in birds.

Materials and Methods

Animals. fUSi was performed in two female carrion crows (*Corvus corone*) from the institute's facility. Crows were housed in small social groups in large indoor and outdoor aviaries (for additional details, see Hoffmann et al., 2011). Crows were provided food and water *ad libitum*. The night before experimental days, crows were fasted for anesthetic purposes. Crow 1 was 1 year old and participated in two sessions separated by 12 d. Crow 2 was 8 years old and participated in a single session. All procedures were conducted in accordance with German and European law and approved by the local authority, the Regierungspräsidium Tübingen.

fUSi. fUSi data were acquired using the Iconeus One system (Fig. 1; Iconeus, Paris, France), specifically designed for animal studies (Bertolo et al., 2021). A linear ultrasonic probe (IcoPrime-15 MHz, Iconeus) was connected to the ultrafast ultrasound scanner system (Iconeus One, 128 channels). The probe, consisting of a linear array of 128 piezoelectric elements with a 15 MHz center frequency and a 0.1 mm pitch, provided a broad field of view (14 mm width, up to 19 mm depth, and 400 μm plane thickness) with an in-plane spatial resolution of 100×100 μm. The size of the probe is $25 \times 17.5 \times 6$ mm ($L \times W \times H$) and weighs ~8 g. The cable

(~2 m in length) extending from the probe is connected to the portable scanner system ($81 \times 73 \times 65$ cm, 90 kg).

The imaging sequence and real-time Doppler reconstruction were performed using a dedicated acquisition software (IcoScan, Iconeus). Two-dimensional (2D) fUSi was performed at a 2.5 Hz framerate where a power Doppler (PD) image was generated every 400 msec. The PD image was generated through a process detailed in Extended Data Figure 2-1 where an ultrasound sequence started with transmitting 11 tilted plane waves (ranging from −10 to 10° in 2° increments) at a pulse repetition frequency of 5.5 kHz. These plane waves form a compound image at a 500 Hz framerate, with 200 compounded images combined in a block. Each block was processed using Singular Value Decomposition clutter filtering to separate tissue signals from blood signals, resulting in the formation of a PD image (Demené et al., 2015).

Surgical procedures. All surgeries were performed while the animals were under general anesthesia. Crows were anesthetized with a ketamine/xylazine mixture (50 mg ketamine, 5 mg xylazine /kg initially and supplemented by 17 mg ketamine, 1.7 mg xylazine /kg, i.m., per hour during the ongoing surgery). After the surgery, the crows received analgesics [butorphanol (Morphasol), 1 mg /kg, i.m.]. The head was placed in the stereotaxic holder that was customized for crows with the anterior fixation point (i.e., beak bar position) 45° below the horizontal axis of the instrument. The skull overlying the brain region of interest was exposed by making an incision along the top of the head through the skin. In birds, the skull is composed of three main layers: the outer cortical bone layer, which is a compact outermost layer; the trabecular bone (spongy layer) beneath the cortical bone; and the compact inner bone layer surrounding the brain. A partial craniotomy (dimensions 18×18 mm) was performed over the left posterior telencephalon, extending across the midline a few millimeters into the right hemisphere. In a partial craniotomy, the outer cortical bone and trabecular bone are removed, while the inner bone layer is left intact. This inner bone layer is thin, allowing for imaging through it without the probe making direct contact with the brain. The same type of partial craniotomy has proven successful for fUSi in pigeons (Rau et al., 2018). The area of interest in the center of the partial craniotomy was the Field L complex, the telencephalic auditory area in birds, which in crows has been localized to 2–3 mm from the midline and 5 mm anterior to the bifurcation of the sagittal sinus (Kersten et al., 2022).

A custom 3D-printed basin (outer dimensions, $24.2 \times 24.6 \times 7.9$ mm; 2.4 g) was attached to the intact bone surrounding the partial craniotomy site with dental cement. During recording, ultrasound transmission gel (Aquasonic, Parker Laboratories) was used to fill the basin in which the probe was positioned and secured. The basin was designed with ridges that allow for the attachment of a fUSi probe holder during recording sessions or a flat cover for after recording sessions to protect the site. The probe holder is a custom 3D-printed part that can be mounted on the basin implant. It slides over the craniotomy interlocking with ridges in the basin implant. It can be secured in place using screws. The probe holder has similar dimensions to the basin implant with additional height ($30 \times 30.8 \times 10.5$ mm) and its weight as 3D-printed polymer is 8.3 g. It has a slot in the inner section that exactly fits the IcoPrime probe. The probe can be moved up and down within this slot to adjust the distance between the probe and inner bone layer to maximize image quality. The basin implant and the probe holder interface in such a way that transmission gel fills the whole space between the two and the probe will always be submerged in transmission gel. The probe is connected with the scanner via a 2-m-long cable. The dimensions of the basin and probe holder are adaptable to experimental needs depending on the brain area(s) to be imaged. After an imaging session, the probe holder is removed, and a basin cover is inserted and held by the ridges of the basin implant.

Angiogram. 3D angiogram recordings of the brain's vasculature were carried out using the integrated "3D angiogram" function of IcoScan with a linear motor stage (SLC-1740, SmarAct, $40 \times 17 \times 8$ mm, 24 g). The linear motor stage was mounted on the stereotactic frame above the partial craniotomy. The motor was only used in the surgical suite

to record the 3D angiogram in the beginning of a session. Another probe holder, especially designed to fit the linear motor stage (provided by Iconeus, $45 \times 20 \times 27$ mm, 12.3 g), was screwed to the motor. This probe holder enabled the motor to move the probe over the craniotomy without the cable getting in the way. The motor-coupled probe could then be moved over the craniotomy in either the mediolateral axis or the anterior–posterior axis to acquire sagittal or coronal scans, respectively. The 3D scan was carried out in step sizes of 0.2 mm. None of the above pieces were attached on the crow's head. For the use of the motor, the earlier mentioned custom 3D-printed probe holder was removed. The basin implant was already secured on the crow's head and ensured that the craniotomy was filled with transmission gel and the probe was submerged in gel during recordings.

The 3D angiogram was performed to gain an overview over the crow brain's vasculature and to examine the image quality, imaging depth, etc. The angiograms are shown in Figure 1, *E* and *F*.

Localization of Field L recording slice. For imaging auditory responses, we positioned the probe in the sagittal orientation, recording a 2D slice with a field of view of 14×19 mm. To determine the best slice to elicit auditory responses, we targeted the region 2–3 mm from the midline. In the surgical suite, a broadband sound was played to the bird for each slice, to ensure the correct probe placement before transferring the bird to the recording setup. The duration of the broadband noise sound was 5 s. The sequence used to test whether there were auditory responses was 5 s of silence→5 s of white noise→5 s of silence. The linear broadband speaker (Visaton SC 13) was placed half a meter away from the crow's head. Ear bars were used to secure the head during surgery but released when sounds were played to find the brain slice containing the highest auditory responses. The fUSi probe was initially secured at the most medial position within the probe holder and then moved via the screw at 1 mm increments laterally.

With IcoStudio, the correlation maps between the stimulus vector and the PD signals were computed. The stimulus vector is a binary vector denoting stimulation with 1 and no stimulation using 0. We expected the neural activity in a primary auditory area to follow the structure of the stimulation. IcoStudio computed correlation maps by correlating the CBV activity of a voxel with the binary stimulus vector, using Pearson's correlation. We noted down which slices showed the highest correlation values with sound presentation and fixed the probe to the slice position with the highest change in CBV and largest area of correlated voxels (Fig. 2*A*; selected 2 mm from midline slice in Crow 2). We then transferred the bird to the acoustic setup with the probe fastened to the basin. Upon arriving in the recording chamber, we immediately checked the position of the probe again by repeating the previous stimulation pattern and continued with planned auditory sequences.

Sound playback and recording apparatus. The experiment was conducted in a dark, ventilated double-walled sound–proof chamber (IAC Acoustics). A linear broadband speaker (Visaton SC 13) played auditory stimuli at an average sound pressure level of 65 dB. The bird was placed in a wire enclosure ($40 \times 40 \times 40$ cm), ~50 cm from the speaker. The chamber was equipped with a camera using infrared LEDs to monitor the bird's behavior throughout the experiment. The crow was able to move around in the closure but did not in darkness; the head position changed a few centimeters during the recording session, and the head did not move relative to the ultrasonic probe. No visible light was used in the chamber.

The Iconeus One system was arranged outside the chamber to allow the probe at the end of the cable to be attached to the bird's head via the probe holder, with sufficient flexibility to accommodate head movements. fUSi acquisition on this system was triggered by the start of an auditory stimulus sequence. For each auditory stimulus sequence file, there are two output channels (stereo; left and right). One channel was fed to the speaker and contained the auditory stimulus that will be played to the crow. The other channel (not sent to the speaker) contained a pure tone pulse that served as trigger for data acquisition and was sent to the Trigger-In port of the IconeusOne scanner system. Data acquisition was therefore aligned with millisecond precision to the start of the sound sequence that the crow heard. The fUSi acquisition came with timestamps which were later aligned to the playback. In generating these

timestamps, the internal acoustic electronic acquisition boards have a jitter of 4 ps root mean square for a 250 MHz clock.

Stimulus sequences. fUSi recordings were performed in two different neurophysiological states. In the anesthetized state, the crows were fully sedated with injections of the ketamine/xylazine anesthetic (i.m., leg muscle), resulting in loss of consciousness, absence of reflexes, immobility, and muscle relaxation. After ~3 h, when the effects of the anesthesia wore off, the crows were imaged in the awake state. We used online video monitoring and direct interaction with the crows between scans to assess behavioral cues such as body position and eye and limb movements to confirm the awake state. The criteria for "awake" were as follows. (1) Eye position and blinking: eyes were open and alert, often showing quick scanning movements. (2) Head movements: birds displayed frequent head movements, including scanning, orienting, and pecking. (3) Posture: an upright posture with smooth, sleek feathers indicated wakefulness. (4) Responsiveness to stimuli: birds responded quickly and reliably to visual, auditory, and tactile stimuli. During this awake state, the crows sat calmly in the darkened, soundproof chamber in quiet rest. For Crow 2, another dose of anesthesia was injected after ~6 h.

In the experiment, we used four distinct stimulus sets to investigate auditory responses. The first set comprised of complex sounds, specifically vocalizations from a crow, pigeon, and canary. A vocalization sequence started with 15 s of silence, 5 s of vocalizations from Bird 1, 15 s of silence, 5 s of vocalization from Bird 2, 15 s of silence, 5 s of vocalizations from Bird 3, and 15 s of silence. So, each vocalization sequence lasted 75 s and with a 2.5 Hz sampling rate, a total of 188 images were acquired. With three different bird vocalization stimuli, a total of six distinct sequences were possible. A total of 20 sequences were presented to the crows drawn from these possible 6 sequences, allowing for 3–4 repetitions of each distinct sequence. The different bird vocalizations varied in frequency content. Recordings (from www.xeno-canto.org) were selected for having low background noise, not containing vocalizations of other birds and having a high recording sampling rate.

Then, pure tones (second stimulus set) and bandpass-filtered noise (third stimulus set) were employed to characterize tonotopic mapping. These stimuli were generated in MATLAB (Version R2023a, MathWorks) using the sin and bandpass functions. The pure tone stimulus set consisted of six pure tones, logarithmically spaced from 250 to 8,000 Hz, covering the hearing range of carrion crows (Jensen and Klokker, 2006). Each pure tone was presented for 5 s, followed by a 15 s silence. A sequence consisted of six tones played in a pseudorandomized order for a total duration of 135 s, including a 15 s baseline period in the beginning of the acquisition. A dataset consisted of a total of 12 pure tone sequences.

The bandpass-filtered noise stimuli set had center frequencies that corresponded to the pure tones in the previous set. The frequency bands increased in width with higher frequencies, ranging from 150 to 300 Hz for the lowest-frequency condition to 4,800–11,200 Hz for the highest-frequency condition. The randomization protocol was the same as for the pure tones.

To determine the response to different stimulus duration, we presented a 1 kHz pure tone for 0.5, 1, and 5 s. This frequency was chosen based on previous experiments, where it elicited a stronger response and is well represented in the crow's auditory system (Jensen and Klokker, 2006). A dataset consisted of each stimulus length played to the crow a total of 16 times.

All sound stimuli were modified to have a 10 ms linear amplitude ramp at the beginning and the end (Woolley and Casseday, 2005; Wagener and Nieder, 2020). This ramping reduces responses to the sharp onset and offset of the stimulus.

Selection of active voxels. Scans, 2D images captured during the playback of different auditory stimuli, were converted to .mat files for further processing. Analyses were conducted using MATLAB (Version R2023a, MathWorks). First, slices in time were corrected with a nonrigid motion correction algorithm (NoRMCorre; Pnevmatikakis and Giovannucci, 2017). After motion correction with NoRMCorre, individual voxels (100×100 μm) were spatially smoothed with a Gaussian kernel of three

voxel widths. Then, for each voxel, the normalized change in cerebral blood volume (ΔCBV) was calculated as a percentage by subtracting the mean baseline value from the trace and dividing the result by the mean of the baseline (Eq. 1):

$$\Delta CBV_t \text{ (in \%)} = \frac{CBV_t - \frac{1}{n}\sum_{k=1}^{n}(CBV_k)}{\frac{1}{n}\sum_{k=1}^{n}(CBV_k)} \quad \Delta CBV \text{ in \%.} \quad (1)$$

The baseline was defined as the period 5 s before stimulus onset up to the onset itself, creating an individual baseline measurement for each auditory stimulation in the trial sequence. To identify active voxels, we first calculated a hemodynamic response function (HRF) by fitting the response to the shortest auditory stimulus we have (500 ms sound) with an inverse gamma distribution (Eq. 2). An inverse gamma distribution has been previously used to fit an HRF computed with fUSi data (Claron et al., 2021). This HRF was very similar to transfer functions calculated between neuronal and vascular response (Aydin et al., 2020, Nunez-Elizalde et al., 2022) and to HRFs used in fMRI (Friston et al., 1994, 1995, Buxton et al., 2004, Lambers et al., 2020):

$$f(t; \alpha, \beta) = A \cdot \frac{\beta^{\alpha}}{\Gamma(\alpha)} \cdot t^{-(\alpha+1)} \exp\left(\frac{-\beta}{t}\right), \quad (2)$$

inverse gamma distribution.

This HRF is convolved with an input signal (i.e., a stimulus vector) to model the underlying hemodynamic response to the auditory stimulus (Friston et al., 1994, Friston et al., 1995, Imbault et al., 2017, Macé et al., 2018, Behroozi et al., 2020, Brunner et al., 2020, Hu et al., 2023, Siegenthaler et al., 2024). This binary stimulus vector shows the on- and off-times of a given stimulus, where, for example, with the 15 s noise bursts sequence used to localize Field L, the 5 s silent baseline before stimulus onset was labeled as 0, and the 5 s noise stimulation phase was labeled as 1, and the 5 s silent off-period afterward was labeled as 0.

The resulting convolved stimulus vector was then used to identify significantly active voxels. To do so, the normalized change in CBV during stimulation was correlated with the convolved stimulus vector using Pearson's correlation, similar to the correlation maps calculated in the IcoStudio software described earlier. To control for multiple comparisons, the Benjamini–Hochberg procedure was applied for false discovery rate (FDR) correction, with voxels showing a corrected p value of <0.001 classified as active.

Activation maps. To visualize the percentage change in CBV activity for significantly active voxels, we overlaid the identified significantly active voxels (as above) with the mean activity during the stimulus period to create average activation maps. We plot the percentage change in CBV for activation maps to the complex bird vocalization, the pure tone, and the bandpass noise stimuli.

Correlation maps. Visualizing the correlation maps for different lengths of stimuli, we computed a convolved stimulus vector for each length of stimulus (0.5, 1, and 5 s). Like the above text on identifying significantly active voxels, for all stimulus lengths, we correlated this vector with the normalized CBV activity 5 s before the onset of the stimulus and 5 s after the onset of the stimulus. The correlation values are shown for significantly correlated voxels.

Frequency maps. We calculated the frequency maps by noting down the frequency which elicited a response for each significant voxel. In cases where a voxel was active for multiple frequencies, we calculated a weighted average from those frequencies (Eq. 3). The weighted average was obtained by normalizing the activity each frequency elicited in the specific voxels to the maximum activity. The normalized activity was then multiplied with the respective frequency. The sum of the multiplied frequencies was divided by the sum of the normalized activity (weights):

$$\text{weighted average} = \frac{\sum (x_i * w_i)}{\sum w_i} \quad \text{weighted average.} \quad (3)$$

Multivoxel pattern analysis (MVPA). We used the Princeton MVPA toolbox (Norman et al., 2006) to conduct the MVPA. The code, originally designed for fMRI datasets, was adapted for fUSi acquisition data files as input and was implemented into a custom script. The MVPA was conducted on the raw acquisition data, i.e., without normalization to the baseline, spatiotemporal smoothing, or preselection of voxels. To account for the delay in the relatively slow hemodynamic response, we shifted the period by 2 s. Only timepoints that fell into the shifted response stimulation period were fed into the MVPA. The input data were z-scored independently for each trial sequence. To divide the data into training and testing data, it was split up into smaller subsets (folds). One such subset consisted of one trial sequence. We used a leave-one-out cross–validation scheme, meaning for each iteration of the classifier, a different fold was withheld to serve as testing data and the remaining folds were used to train the classifier. The classifier was run several times, so that each fold was used as testing data once. In each iteration, a feature selection using an ANOVA with a $p < 0.05$ threshold was performed. Each voxel is a feature. Since we had 20,864 possible features and not all of them responded to auditory stimulation, feature selection was important to reduce the input of unnecessary data. The ANOVA selected voxels which were significantly different between the conditions. This feature selection was performed only on the training data and individually for each iteration to ensure that no bias was introduced by manually selecting active voxels. In each iteration, a backpropagation classifier with 10 hidden layers was trained on $n-1$ scans as training data and 1 scan as testing data. We report the mean accuracy and standard error of the classifiers.

Statistics. A series of statistical tests were used to further analyze the data. A one-sample t test confirmed that classification performance differed from the chance level. A one-way ANOVA was used to identify significant tuning of example voxels. A paired two-sample t test was used to compare the number of active voxels between anesthetic states, and a separate two-tailed two–sample t test examined differences in classification accuracy between these states.

Results

fUSi was performed in two crows. We positioned the ultrasound probe (IcoPrime-15 MHz, Iconeus) along an anterior–posterior axis above the partial craniotomy window; the region covered includes the auditory telencephalon termed the Field L complex (Fig. 1A,B). The partial craniotomy covered most of the posterior left hemisphere, crossing slightly over the midline into the right hemisphere. A custom-designed basin implant and probe holder above the partial craniotomy were used to localize and fix the position of the probe on top of the crow's head (Fig. 1C). The probe imaged a 2D brain slice with dimensions of 14 mm anterior–posterior by 19 mm dorsoventral (Fig. 1D,E).

The first step was to image the brain structures beneath the partial craniotomy. Using a linear motor stage (SLC-1740, SmarAct motor) to precisely move the ultrasound probe from medial to lateral in 200 μm steps, we acquired a 2D image at each position. The high spatial resolution of ultrasound imaging enabled detailed depiction of even fine blood vessels branching from the major vessels, which predominantly run along the dorsoventral axis (Fig. 1D,E). These individual 2D images were graphically combined to create a 3D image of the brain volume (Fig. 1F,G) that reveals the fine details of the brain vasculature network.
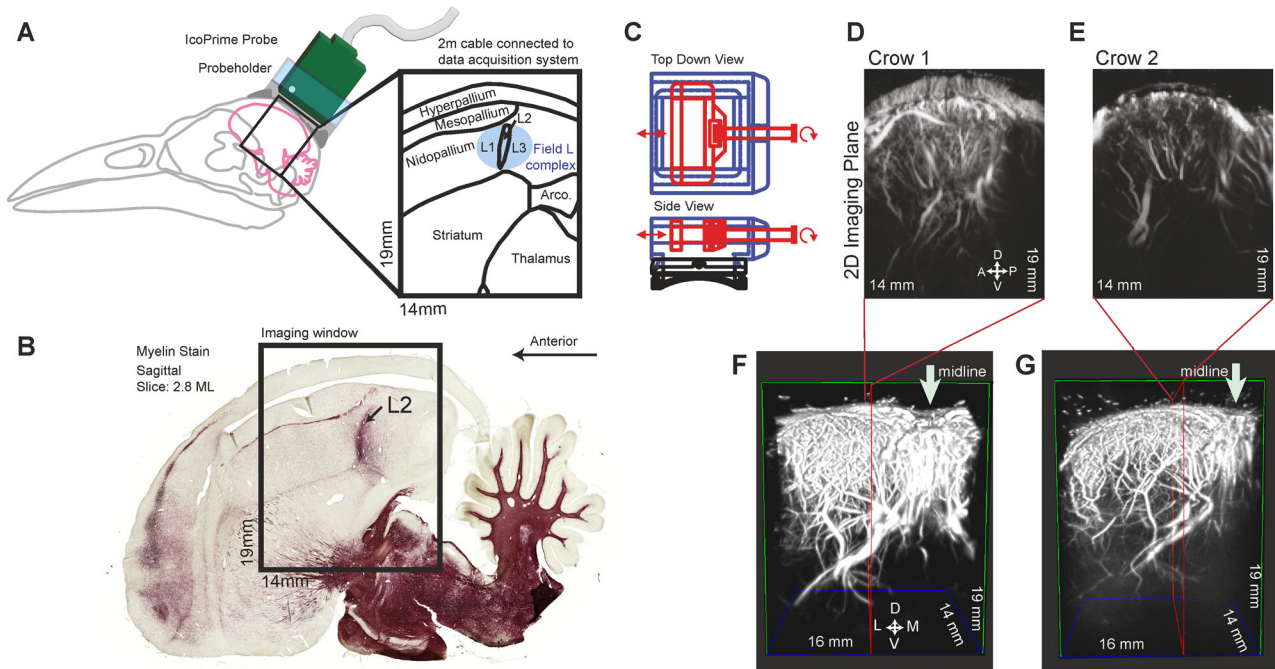
Figure 1. Ultrasound imaging of the posterior telencephalon in the crow. *A*, A diagram of the carrion crow skull and brain showing the green ultrasound probe (IcoPrime) positioned over the posterior half of the telencephalon with basin implant and removable probe holder (in blue). The black rectangular outline represents the imaging window (14 × 19 mm) extending into the brain. The connected inset shows the magnified schematic of the anatomical structures found within the imaging window. The avian auditory telencephalon, specifically the Field L complex, is shaded in blue. *B*, Sagittal histological section of a crow brain (2.8 mm lateral from the midline—adapted from the Crow Brain Atlas by Kersten et al., 2022) stained for myelin reveals the L2 subregion of the Field L complex. The fiber characteristics of the L2 subregion arise from dense thalamic input from the nucleus ovoidalis. *C*, The diagram of the basin implant (black) with removable probe holder (blue) with movable inner section (red). The inner section holds the probe and can be moved horizontally using a screw to change the imaging site. The probe holder (blue) slides into ridges in the side of the basin implant and is secured with screws during use. On top is a top–down view, and the bottom is the side view. The dimensions of the basin and probe holder are reported in Materials and Methods. *D*, A 2D angiogram (visualization of blood vessels) for Crow 1, acquired from the imaging window depicted at the coordinates outlined in *A* and *B*. *E*, 2D angiogram for Crow 2. *F*, A 3D angiogram of the left hemispheric posterior telencephalon of Crow 1, mildly extending across the midline (indicated by a downward-pointing arrow) into the left hemisphere. This image displays the brain volume beneath the partial craniotomy window, generated by graphically combining 2D images (one scan every 200 μm in mediolateral extension), as shown in *D* and *E*. *F*, 3D angiogram of Crow 2.

Functional localizer protocol

To test for auditory-related changes in CBV to localize the putative avian auditory telencephalon (i.e., the Field L complex), we used an auditory localizer protocol applied to anesthetized crows. The ultrasound probe was moved in the mediolateral direction in 1 mm steps within the area of the partial craniotomy. At each position, auditory noise bursts (5 s duration, surrounded by 5 s of silence) were presented to test for stimulus-correlated changes in CBV. Online, using dedicated software (IcoStudio), CBV responses for each voxel were correlated with the stimulus vector (noise sound) to create correlation maps (Fig. 2A). We visualized correlated CBV responses by thresholding activity to 20% to see which slices contained the most correlated responses.

In Crow 2, a slice 2 mm lateral from the midline showed a pronounced activated region at a location that coincided with the core of the Field L complex, as predicted by neuroanatomical coordinates (Kersten et al., 2022; Fig. 2A, middle panel). Within this region of activation, the CBV increased sharply ∼2 s after the physical sound onset, reached a plateau of roughly 25% signal increase (100% signal change indicates that CBV has doubled compared with the baseline), and returned to the baseline with a delay comparable to the onset delay (Fig. 2C). In a region outside of this "hot spot," but neighboring it, the CBV remained at the baseline throughout sound stimulation (Fig. 2B). Slices positioned more medially or laterally showed less stimulus-correlated CBV activation. The slice with the most pronounced activation during the functional localizer protocol (2 mm lateral from the

midline in Crow 2, 3 mm lateral from the midline in Crow 1) was used to secure the probe at that particular location to be subsequently used for the following stimulation protocols, measurements, and analyses.

Responses to bird vocalizations

To test whether the CBV changes were specific and robust enough to represent complex sounds, we employed a block design with playbacks of three different acoustically rich vocalizations from a crow, a pigeon, and a canary. The vocalizations were intensity-equalized but naturally differed in other acoustic dimensions, such as frequency range (Fig. 3A; pigeon, low frequencies; crow, middle frequencies; canary, high frequencies). Each call sequence consisted of 5 s intervals of each repeated vocalization, with 15 s of silence between each vocalization block.

Figure 3A shows four repetitions of one vocalization sequence and the temporally correlated CBV traces obtained from an example voxel indicated in Figure 3B. The CBV changes align with the stimulation onsets, with the largest CBV responses occurring during pigeon vocalizations. CBV responses for each voxel were correlated with the hemodynamic response convolved stimulus vector ($p < 0.001$, FDR corrected) for each bird vocalization to generate the mean activity map. The pigeon map is shown in Figure 3B where the resulting activation was located primarily in a dorsal region.

Figure 3C shows four repetitions of the same vocalization sequence as above and the temporally correlated CBV traces
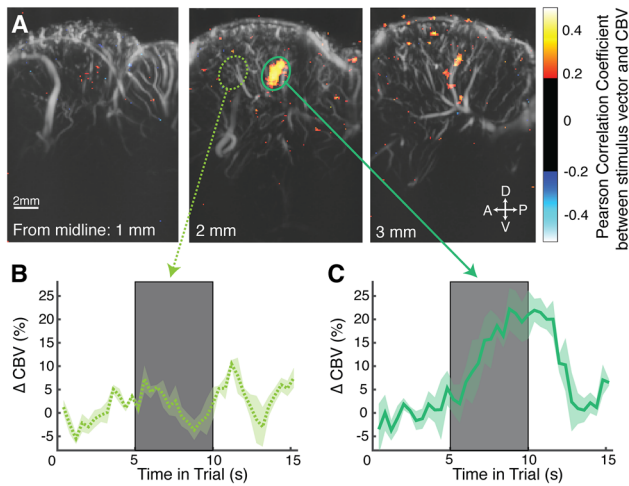
Figure 2. Localizer protocol for auditory activity in anesthetized crows. *A*, fUSi was performed while stimulating with noise bursts (sequence, 5 s silence→5 s white noise→5 s silence) and moving the probe from medial to lateral. PD images from brain slices in Crow 2 at 1, 2, and 3 mm lateral to the midline are shown as examples. The creation process of PD images is illustrated in Extended Data Figure 2-1. The middle slice, at 2 mm lateral from the midline, shows a pronounced correlation of the CBV signal with the noise stimulus in a brain region that coincides with the Field L complex depicted in Figure 1, *A* and *B*. *B*, Example CBV trace (in percentage relative to the silence baseline) during a noise burst in a region at slice 2 mm lateral from the midline that showed no stimulus-correlated change. This activity trace is taken from the brain region in *A* (middle) indicated by a dotted light green circle. The gray area marks the noise stimulation period. *C*, Example CBV trace during a noise burst at the same slice that is stimulus correlated. This activity trace is taken from voxels in the brain region indicated by a solid green circle. The shaded area indicates the standard error of the mean (SEM) across three repetitions of the noise burst sequence.

obtained from an example voxel indicated in Figure 3D, which was most responsive to crow vocalizations. The activation map for crow vocalizations (Fig. 3D) was located more ventrally compared with the map for pigeon vocalizations (Fig. 3B). Similar regionally different activation patterns were seen in Crow 2 to pigeon vocalizations (Fig. 3E) and crow vocalizations (Fig. 3F).

Next, we applied machine learning classifier analyses to the fUSi data. Specifically, we performed a MVPA to infer the type of auditory responses in the imaged brain area. MVPA is a supervised classification technique used to identify relationships between spatiotemporal patterns of fUSi activity and stimuli conditions. Figure 3G shows the classifier performance (plotted as a confusion matrix) in predicting vocalizations based on data recorded from Crow 1 averaged over 20 iterations. The accuracy, i.e., the proportion with which the classifier correctly predicted a vocalization condition, is shown along the main diagonal of the confusion matrix. The classifier accuracy for Crow 1 is at $92.3 \pm 3.27\%$ and thus significantly above the chance level of 33% correct classification, given the three possible vocalization conditions (one-sample t test; $p < 0.001$; $t_{(19)} = 18.011$). For Crow 2, the classifier was also able to predict all three vocalizations with above-chance accuracy (mean, $64.6 \pm 3.48\%$; one-sample t test; $p < 0.001$; $t_{(19)} = 8.981$; Fig. 3H).

These data demonstrate that the CBV changes measured with fUSi were specific and robust enough to represent complex sounds. Moreover, the distinct activation locations of the bird vocalizations along the dorsoventral axis suggest that different sound frequencies within the vocalizations (Fig. 3I) activate specific regions of the auditory telencephalon. Based on this,
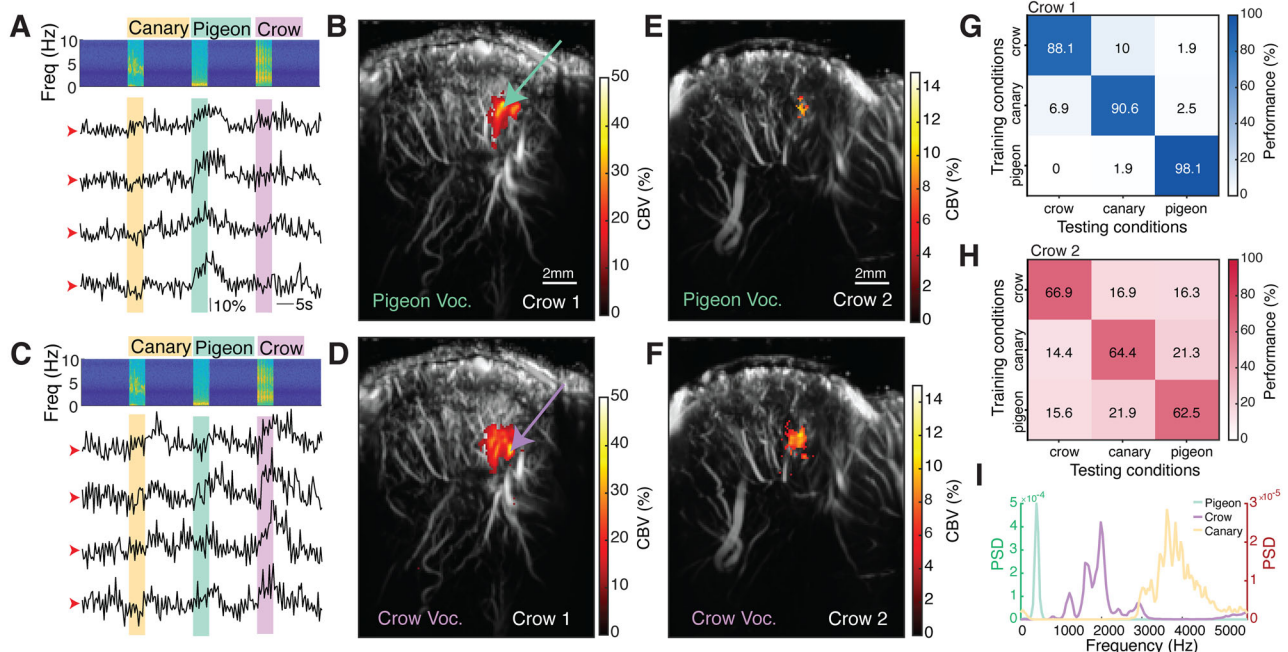

Figure 3. Mapping CBV changes in anesthetized crows to playback of complex bird vocalizations. *A*, Example bird vocalization stimulation sequence and corresponding CBV changes from an example voxel responsive to pigeon sounds in Crow 1. The top panel shows the spectrogram of one sequence of bird vocalizations (canary, pigeon, crow). The four bottom traces depict the single-trial CBV responses from four repetitions of this particular sequence. The red arrows indicate 0% change in CBV. The CBV traces were taken from a voxel at the tip of the green arrow in *B*. *B*, Mean activation map in Crow 1 for pigeon vocalizations (green stimulus interval shown in *A*). *C*, Vocalization sequence and corresponding CBV changes from a voxel responsive to crow sounds. The CBV traces were taken from a voxel indicated by the tip of the purple arrow in *D*. *D*, Activation map for crow vocalizations (purple stimulus interval shown in *C*). *E*, Activation map for pigeon vocalizations in Crow 2. *F*, Activation map for crow vocalizations in Crow 2. *G*, Confusion matrices showing the performance of an MVPA classifier predicting the type of bird vocalization played based on voxel activity for Crow 1 (in blue). *H*, Confusion matrices showing the performance of an MVPA classifier for Crow 2 (in red). *I*, Frequency content of different bird vocalizations (pigeon in green, crow in purple, and canary in yellow). The curve for pigeon vocalizations corresponds to the left power spectral density (in green), while the curves for crow and canary vocalizations correspond to the right PSD (in red).

we next investigated the tonotopic mapping within the Field L complex in greater detail.

Tonotopic mapping in awake crows using pure tones

For the investigation of tonotopic mapping, we presented the crows with six pure tone sounds of equal intensity, with frequencies increasing in 1 octave steps (250, 500, 1,000, 2,000, 4,000, and 8,000 Hz). These frequencies are known to cover the typical hearing range of crows and other songbirds (Dooling et al., 2000; Jensen and Klokker, 2006). The six sounds were presented for 5 s each in a pseudorandomized order in each scan (Fig. 4A). After each sound, 15 s of silence followed. Figure 4A shows example CBV traces averaged over nine voxels in the Field L complex. The responses to specific sound frequencies (indicated by color bars) were similar between scans. For further analysis, the traces were aligned at the onset of the stimulation period, with the 5 s before stimulation onset taken as the individual baseline.

We calculated the normalized activity of each voxel for each sound frequency presentation. The resulting change in CBV is relative to the baseline and can therefore be compared across all voxels and conditions. The mean activity map was calculated for each frequency presented to Crow 1 (Fig. 4B). The spatial distribution of active voxels changed with each of the six stimulus frequencies: low-frequency stimuli elicited a response in more dorsal–posterior areas, while higher-frequency stimuli elicited a response in more ventral–anterior areas of the Field L complex (Fig. 4B).

We next calculated a frequency map from these activity patterns in Crow 1 (Fig. 4C). To do this, we superimposed activity for each sound frequency, using different colors to represent the individual frequencies. In cases where a voxel was active across multiple frequencies, we calculated the weighted average frequency resulting in a detailed frequency map showing clear tonotopy, with a systematically ordered spatial representation
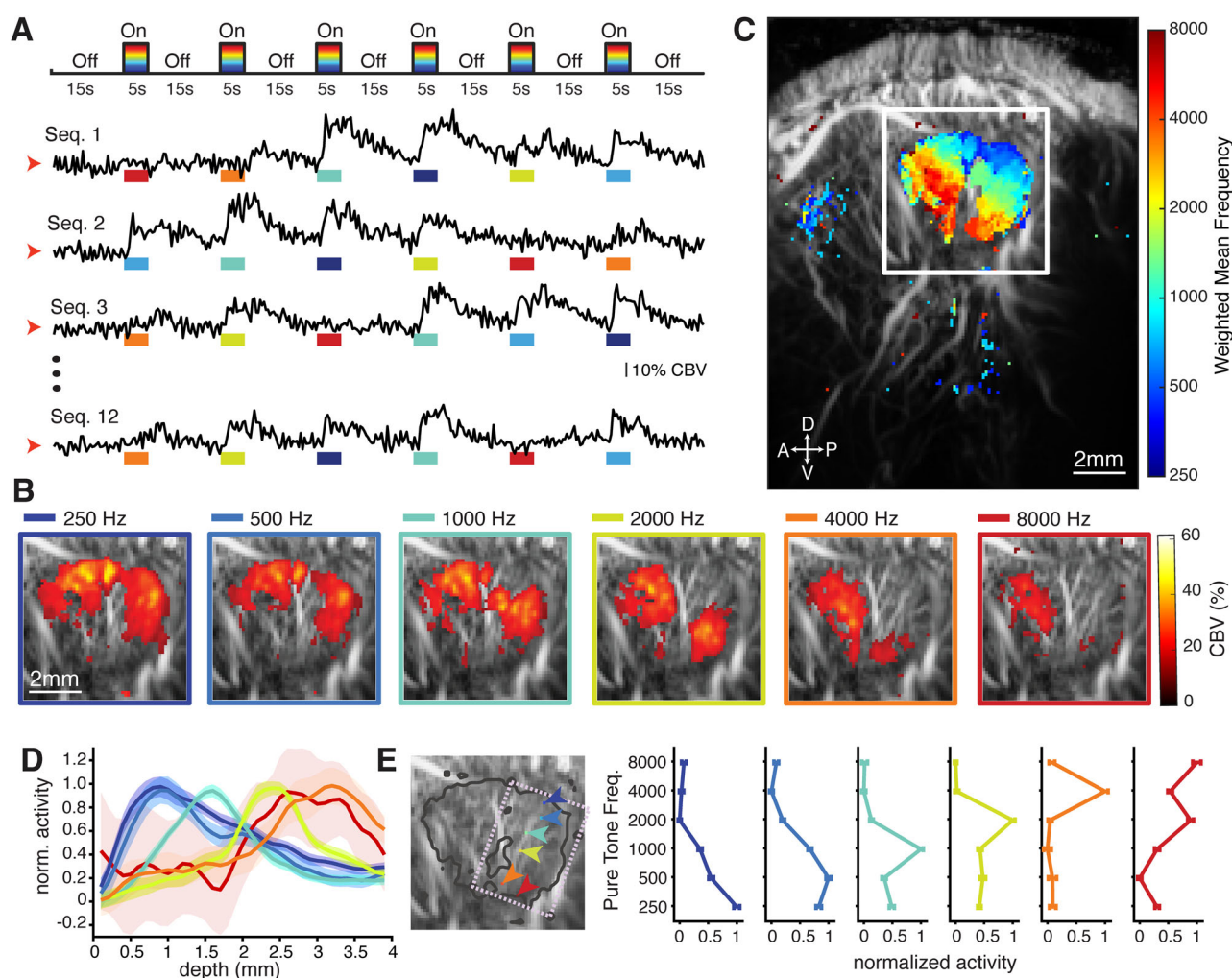

Figure 4. Topographic arrangement of pure tone representations in awake crows. **A**, The top panel schematic shows the pure tone sequence, consisting of six sequential pure tones (5 s duration) of systematically varying frequencies (color coded) separated by silence (15 s duration). The CBV traces below are from voxels in the Field L complex during four example scans temporally aligned to the sound sequence. Color bars indicate sound frequency presented (navy, 250 Hz; blue, 500 Hz; teal, 1,000 Hz; chartreuse, 2,000 Hz; orange, 4,000 Hz; red, 8,000 Hz). The red arrows indicate 0% change in CBV. **B**, Average activation maps in Crow 1 (graphically zoomed in on the Field L complex; see white square in **C**) arranged in increasing sound frequencies from left to right. The color of the frames indicates the sound frequency. **C**, Tonotopic frequency map, activation to each sound frequency was superimposed and used to compute a weighted average, with cool to warm colors representing increasing sound frequencies. Similar tonotopic frequency maps are shown for bandpass-filtered noise stimuli in Extended Data Figure 4-1. **D**, Isointensity frequency tuning curves of the voxels along the dorsoventral imaging depth axis (depth in millimeters aligned to the dorsal short edge of dotted lavender rectangle in **E**). CBV activity was normalized to each frequency's maximum response. The shaded area indicate SEM. **E**, Zoomed-in square of the Field L complex [significant voxel cluster outlined in black (n = 1,193 voxels), the area analyzed in **D** in dotted lavender rectangle] with example voxels to the right indicated at the point of the colored arrows. Next to image, the six example voxels are shown with tuning for a particular frequency. Error bars indicate SEM.

of sound frequencies (Fig. 4C). Only a cluster of voxels near the middle showed no positively correlated activity, separating the otherwise coherently connected topographic map in the Field L complex. To further visualize the topographic mapping, we plotted the average activity for each frequency along the dorsoventral axis of the target region (Fig. 4D). These isointensity curves (same acoustic sound pressure level across measurements) show that the location of maximum activity differs between frequencies. Example voxels ($n = 6$; Fig. 4E) were selected for having the highest change in CBV for each respective pure tone frequency. We performed a one-way ANOVA to determine if the activity of these selected voxels differed between the presented frequencies. For all example voxels, except for the rightmost voxel, the activity elicited by the different frequencies differed significantly (one-way ANOVA; $p < 0.001$). For the rightmost voxel, the activity did not differ significantly between frequencies (one-way ANOVA; $F_{(5,66)} = 1.66$; $p = 0.1553$—generally, the responses elicited by the 8,000 Hz condition were lower than for the other lower frequencies).

This procedure and analyses were repeated using six bandpass-filtered noise bursts that systematically increased in frequency from 150–350 Hz to 4,800–11,200 Hz. The tonotopy observed for pure tones could similarly be retraced with bandpass-filtered noise (Extended Data Fig. 4-1). There was a dorsoventral organization of increasing frequencies.

Comparison of anesthetized and awake states

Dramatic differences in CBV responses to pure tones and bandpass noise bursts were observed when the crows were awake compared with when they were deeply anesthetized (neurophysiological states). Figure 5A shows the weighted frequency map calculated when Crow 1 was deeply anesthetized and Figure 5B is when it was more awake. These changes of CBV were not related to slow drifts in signal over time but were a consequence of the physiological state (Extended Data Fig. 5-1). To compare the number of active voxels between stimulus types, neurophysiological states, and individual birds, we considered a voxel to be active if its CBV changes correlated significantly with the stimulus vector.

To investigate the influence of neurophysiological state on the number of active voxels, we counted the number of voxels for each condition (six frequencies, 250–8,000 Hz) and stimulus types (pure tones and bandpass-filtered noise) for each bird. This resulted in 12 samples for both the anesthetized state and the awake state. For Crow 1, an average of $1,801.6 \pm 217$ voxels were active in the awake state, which was significantly more than the 92.2 ± 16.1 active voxels in the anesthetized state (paired t test; $t_{(11)} = 8.2$; $p < 0.001$; Fig. 5C). In Crow 2, although there were fewer active voxels in total, the difference between the neurophysiological states was also significant (paired t test; $t_{(11)} = 3.28$; $p = 0.007$; Fig. 5D). In the awake state, we found on average 273.6 ± 78.6 voxels, while we found only 19.5 ± 6.6 active voxels in the anesthetized state. Anesthesia clearly led to a reduced overall activity in both birds. Analyzing the same active voxels across both neurophysiological states, we found an overall reduced CBV response during anesthesia (Crow 1, paired t test; $t_{(687)} = -33.68$; $p < 0.0001$; Crow 2, paired t test; $t_{(54)} = -5.95$; $p < 0.0001$) and no change in the variability in responses (calculated as the coefficient of variance—Crow 1, paired t test; $t_{(10)} = -1.61$; $p = 0.1379$; Crow 2, paired t test; $t_{(6)} = 1.45$; $p = 0.1960$) across states.

Next, we used MVPA to gain more insight into the stability of the frequency mapping. Since MVPA allows us to use the whole im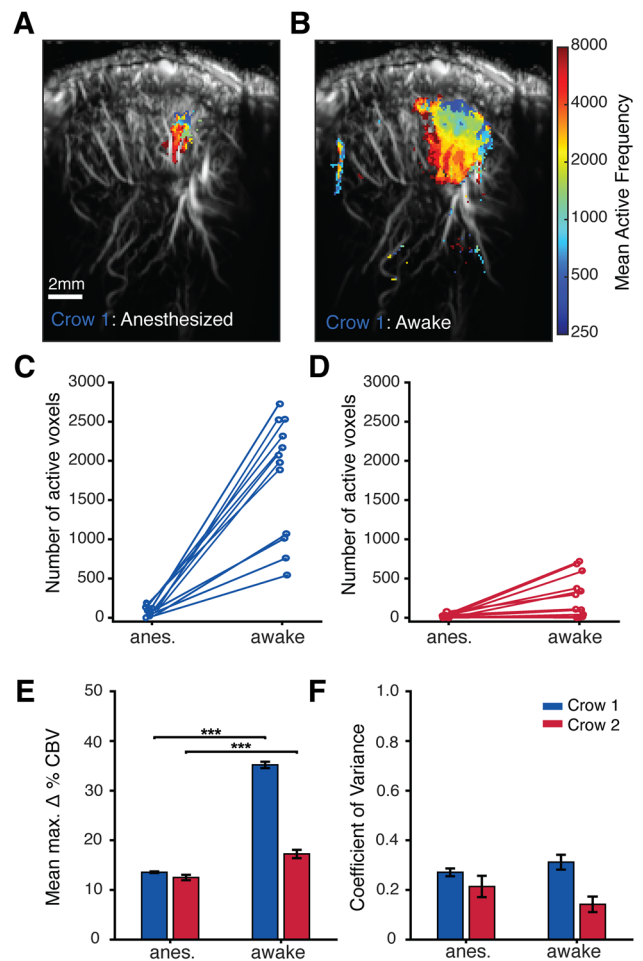age without preselecting active voxels, it provides a more agnostic analysis approach by utilizing more subtle changes in activity patterns to classify conditions. This makes it particularly useful for datasets with less overall activity. Additionally, since we observed tonotopic mapping in both the anesthetized and awake states, one key question we aimed to resolve was whether this tonotopic pattern was consistent across neurophysiological states. The confusion matrices (Fig. 6A–D) show the accuracy with which the classifier predicted conditions for Crow 1 averaged over 12 iterations. Given that there are six frequencies, the chance level is 16.7%.

Overall, the classifier demonstrated above-chance accuracy in predicting the pure tone frequencies for Crow 1 (one-sample t test; $p < 0.001$; Fig. 6E,F). It achieved an accuracy of $41.2 \pm 4.5\%$ when trained and tested on the anesthetized data (Fig. 6A). Accuracy varied depending on the neurophysiological state,

Figure 5. Comparison of auditory activation during neurophysiological (awake vs anesthetized) states. **A**, Tonotopic frequency map for Crow 1 under anesthesia. **B**, Tonotopic frequency map for Crow 1 when awakened. **C**, The number of active voxels in the two different neurophysiological states for Crow 1. Each jittered point represents one combination ($n = 12$ per state) of stimulus type (2; pure tones, bandpass noise) and stimulus frequency (6; 250, 500, 1,000, 2,000, 4,000, 8,000 Hz). Lines connect the pairs of the same stimulus condition in the two different neurophysiological states. **D**, The number of active voxels in each neurophysiological state for Crow 2. **E**, Difference of the average maximum amplitude (Δ% CBV) during stimulation between the two neurophysiological states (anesthetized and awake) in voxels that are significantly active both in the anesthetized and the awake states. The color indicates crow identity (blue, Crow 1; red, Crow 2). Error bars indicate the SEM. *** = $p < 0.001$. **F**, Coefficient of variance (CV) in both anesthetized and awake states in the same voxels as in **E**. Extended Data Figure 5-1 shows changes in CBV activity result from differences in neurophysiological state and are not due to drift through time.
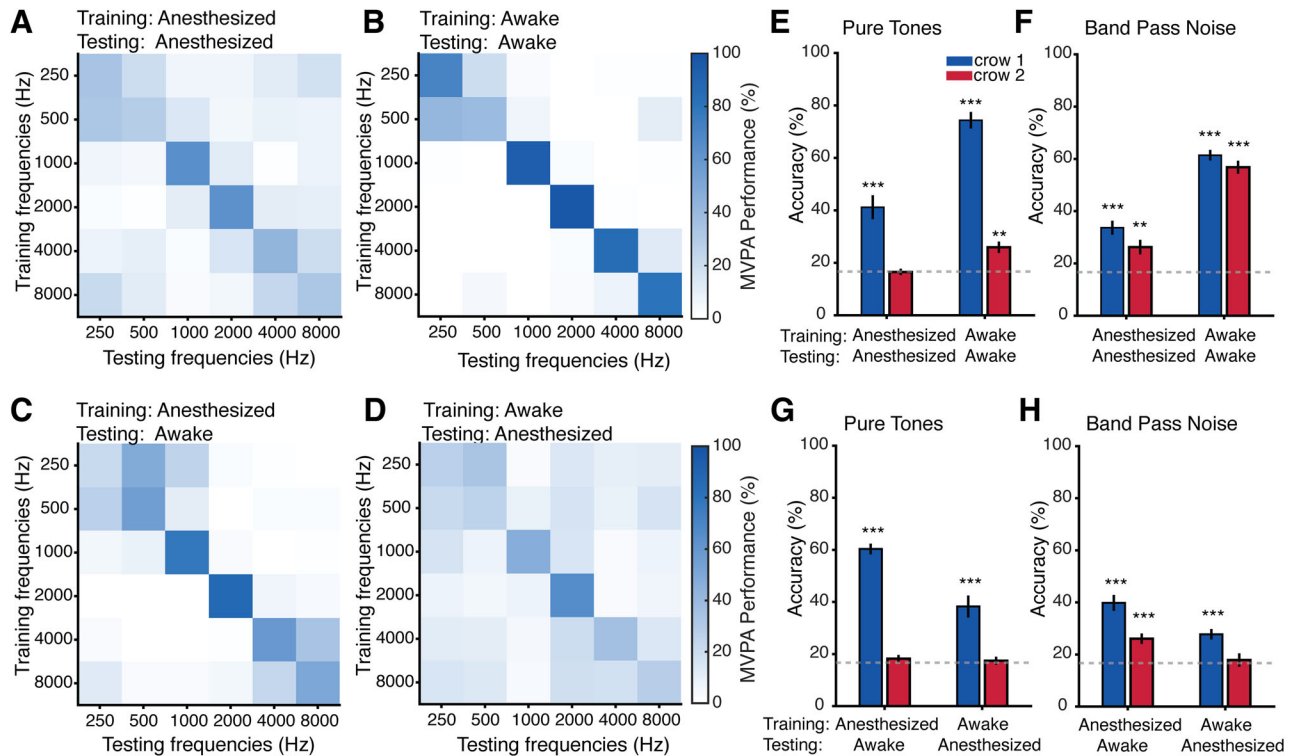
Figure 6. Patterns of voxel activity reveal frequency tuning within and across neurophysiological (awake vs anesthetized) states. ***A***, Confusion matrix displaying the accuracy of an MVPA classifier when predicting the frequency of pure tones played to the anesthetized Crow 1. ***B***, Confusion matrix for the awake Crow 1. ***C***, Across-neurophysiological state confusion matrix of the MVPA classifier trained on dataset from the anesthetized Crow 1 and tested on data from the awake Crow 1. ***D***, Across-neurophysiological state confusion matrix of the MVPA classifier trained on data from the awake Crow 1 and tested with data from the anesthetized Crow 1. ***E,F***, Overall accuracy of within-neurophysiological-state classifiers for pure tone (***E***) and bandpass noise stimuli (***F***). The gray line indicates the chance level for the MVPA classifiers given six different sound frequencies. Color indicates crow identity (blue, Crow 1; red, Crow 2). ***G,H***, Overall accuracy of across-neurophysiological state classifiers for pure tone (***G***) and bandpass noise stimuli (***H***). Error bars indicate the SEM. *$p < 0.05$; **$p < 0.01$; ***$p < 0.001$.

with the highest accuracy observed for the awake–awake condition at 74.4 ± 3.1% (Fig. 6B). Overall, the classifier was able to predict conditions significantly above chance when tested within the same neurophysiological state (Fig. 6E,F). The only exception was the classifier trained and tested on the dataset for pure tone stimulation under anesthesia in Crow 2 ($t_{(11)} = -0.129$; $p = 0.9$).

The classifiers also generally performed well in predicting sound frequencies when trained across neurophysiological states for Crow 1 (Fig. 6G,H; one-sample t test; $p < 0.001$). For the classifier trained on the anesthetized dataset and tested on the awake dataset, accuracy was 58.7 ± 3% (Fig. 6C), while the accuracy dropped to 38.3 ± 4.2% for the classifier trained on the awake dataset and tested on the anesthetized dataset (Fig. 6D). In Crow 2, fewer active voxels were observed, and the changes in CBV relative to baseline were less pronounced. The effect of this reduced activity compared with Crow 1 is also reflected in the classification accuracy for Crow 2. For Crow 2, the only across-neurophysiological state classifier that could predict conditions above chance was the one trained on the bandpass noise dataset under anesthesia and tested on the awake dataset (Fig. 6H; $t_{(11)} = 4.723$; $p < 0.001$).

Effect of stimulus length on CBV changes
Stimulus durations in cognitive tasks are typically shorter than our previously applied 5 s stimuli. We therefore explored CBV responses to three different stimulus durations (5, 1, and 0.5 s) of the same frequency stimulus (1,000 Hz pure tone).

We first examined significant correlation maps with a threshold of $p < 0.001$, FDR corrected (Fig. 7A) for stimuli lengths of 0.5, 1,

and 5 s, respectively. The correlation maps were robust and similar between the shorter stimuli lengths (0.5 and 1 s) compared with the longer stimulus length of 5 s. We selected five voxels (Fig. 7A, at the tip of the colored arrowheads) and plotted their CBV traces (Fig. 7B). CBV responses could be detected for short 0.5 and 1 s stimulations; the magnitude and length of elicited responses were similar between the shorter stimulation lengths. For the two shorter stimulus lengths, CBV increased after stimulation onset to a peak that shortly decayed. Interestingly, the responses differed with the longer 5 s stimulation duration. In Figure 7B, the example voxels (orange, blue, and navy arrowheads) had sustained activity throughout the entire stimulation period and past the offset of the sound. Another example voxel (yellow arrowhead) had a short increase in CBV before a larger, longer negative deflection. The middle example voxel (magenta arrowhead) showed a transient positive response at the onset and the offset of the stimulus. This diversity of responses suggests that fUSi could be used to examine putative functional subfields within the Field L complex that show different CBV changes with time.

To examine these dynamics, we superimposed the CBV value for each voxel that passed a threshold of 5% change from the baseline for each fUS image (0.4 s duration), starting from 0.8 s before stimulus onset to 1.4 s after the end of the 5 s sound (Fig. 8). Different patterns of activity emerge during the onset, maintenance, and offset of the 5 s sound stimulus. For the first few frames after stimulation onset, there is a positive increase throughout the Field L complex. After ~2 s, the region appears to divide with two flanking robust sustained positive responses and a middle region that experiences a negative deflection. After the offset of the
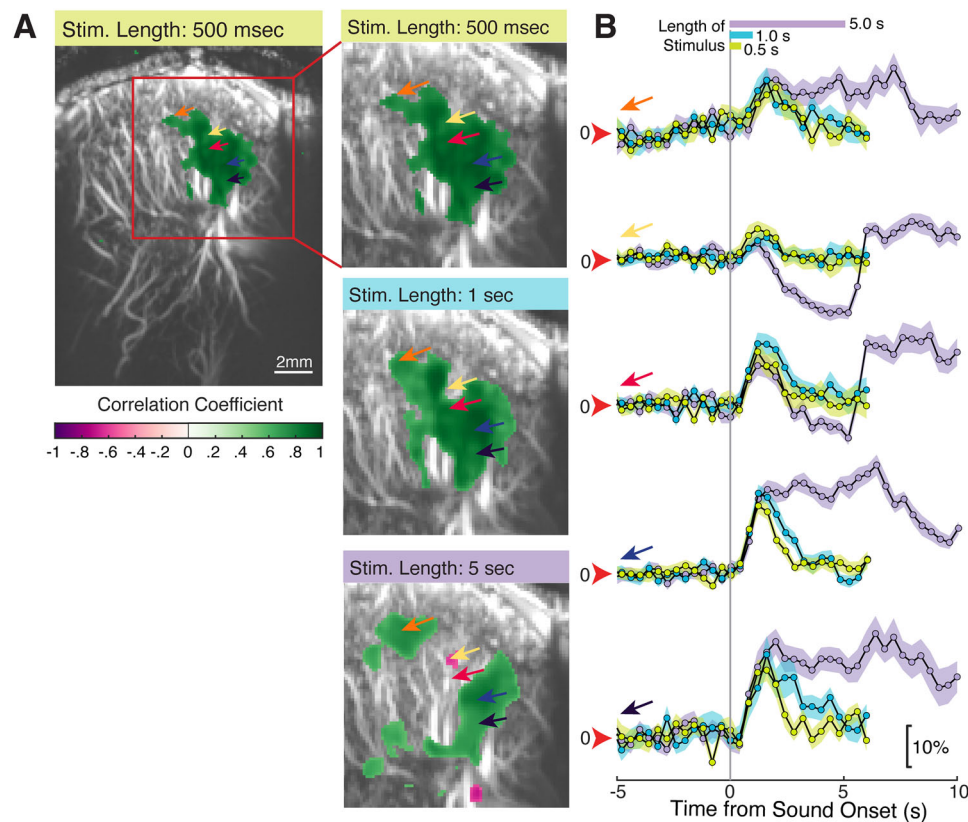
Figure 7. Auditory responses in the Field L complex of an awake crow are scaled by length of stimuli presented. **A**, Correlation map of active voxels to a 0.5 s stimulus (green; pure tone, 1,000 Hz). Positive correlations are in green and negative correlations in pink. The five colored arrowheads indicate voxels at the point that have associated CBV traces plotted in **B**. To the left is a magnified window centered around the Field L region. This window is also shown for the correlation maps to a 1 s stimulus and a 5 s stimulus. **B**, The activity (CBV traces) of the corresponding voxels indicated by the colored arrowheads in **A** for playback of a 0.5 s (green), 1 s (blue), and 5 s (purple) sound stimulus. The red arrows indicate 0% change in CBV. Note the differing length of CBV traces is due to the addition of 5 s of scan time poststimulus offset. The shaded area indicates SEM.

stimulus, this negative deflect reduces and the divisions appear to merge again into a cluster of positive activity. This visualization suggests that different response dynamics could indicate finer spatial organization within the Field L complex.

Discussion

Applying fUSi to crows, we investigated Field L responses to complex vocal stimuli, revealing a spatial organization informative of the stimuli's frequency content. A fine-scale topographic analysis showed robust tonotopic mapping along the dorsoventral axis of the Field L complex. Notably, this tonotopic organization persisted across neurophysiological states, as revealed by cross-state MVPA analyses. Visualizing responses to long and short stimuli in a time-resolved manner revealed region-specific response patterns that could delineate putative subregions.

This study represents the first application of fUSi to investigate the songbird brain. Rau et al. (2018) demonstrated the feasibility of fUSi in birds, localizing the pigeon visual wulst, entopallium, and the Field L complex. Here, we provide a detailed investigation into the dynamics of the Field L complex's response properties using diverse auditory stimuli, including naturalistic and frequency-controlled sounds, compared across neurophysiological states.

Methodological considerations

Our procedures left the inner bone layer intact while achieving high-quality imaging, allowing us to reconstruct detailed tonotopic maps with few scans. We could efficiently map auditory stimuli responses in ~15–30 min, enabling us to examine the effect of anesthesia on frequency representations in one session. CBV signal amplitudes obtained from crow fUSi were ~25% and thus large compared with typical fMRI BOLD responses (Boido et al., 2019). Similarly, auditory CBV responses have been reported to be ~20–30% (Bimbard et al., 2018, Takahashi et al., bioRxiv) compared with typical auditory cortex BOLD responses of ~5%. However, fUS images are 2D. 3D imaging (Gesnik et al., 2017, Rau et al., 2018, Rabut et al., 2019, Brunner et al., 2020, Bertolo et al., 2021) currently require heavier motors or larger probes, precluding head-free protocols. Lightweight volumetric probes are actively being developed.

Currently, fUSi allows a wide field of view and high spatiotemporal resolution to image brain dynamics underlying complex behaviors. This has led to its application to diverse species: mice (Macé et al., 2011, Boido et al., 2019, Aydin et al., 2020, Brunner et al., 2020, Bertolo et al., 2021, Edelman et al., 2021), rats (Sieu et al., 2015, Urban et al., 2015, Tiran et al., 2017, Rabut et al., 2019, El Hady et al., 2024), macaques (Dizeux et al., 2019, Norman et al., 2021, Claron et al., 2023, Griggs et al., 2024), marmosets (Takahashi et al., bioRxiv, Zhang et al., 2022), ferrets (Bimbard et al., 2018, Hu et al., 2023), pigeons (Rau et al., 2018), and newborn and adult humans (Demene et al., 2017, Imbault et al., 2017, Rabut et al., 2024). Critically, fUSi can be performed in awake and freely moving animals—making it a highly attractive technique to study the complex cognitive and communicative behaviors of corvids.
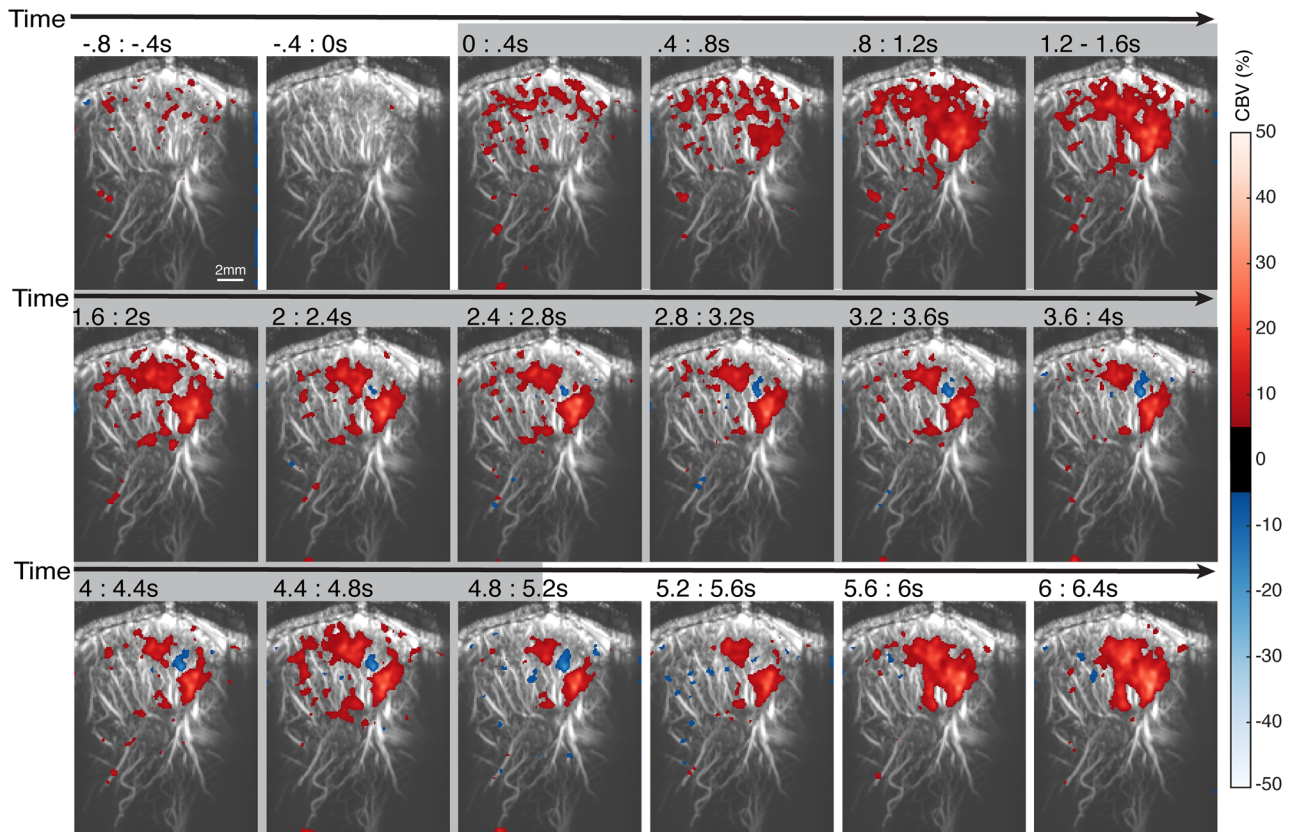
Figure 8. Dynamics of auditory responses in the Field L complex of an awake crow to a 5 s stimulus. Each fUS image spanning a stack of compound images over 0.4 s is plotted from two images before the onset of the sound stimulus to three images after the offset of the sound stimulus for Crow 1. The percentage change in CBV (thresholded by 5%) is plotted for each image. Different patterns of activity emerge during the sound stimulus (as marked by the gray background) and afterward as images progress through time from left to right along each row. Positive CBV changes are colored in red, and negative CBV changes are colored in blue (dimensions of individual frames as in Fig. 1D).

CBV changes in the auditory telencephalon

The physiology of the auditory telencephalon in corvids was underexplored. The Field L complex is the primary avian auditory area, functionally analogous to the mammalian primary auditory cortex (Elliott and Theunissen, 2011). In our study, we observed sound-induced CBV changes in the posterior telencephalon. The anatomical coordinates of these changes aligned with those of the Field L complex, reported in histological studies (Kersten et al., 2021; 2022; 2024). Additionally, this location corresponds to regions where neuronal activity in response to simple and complex sounds has been recorded in other songbirds (zebra finches, Gehr et al., 1999; Calabrese and Woolley, 2015; starlings, Müller and Leppelsack, 1985; Rübsamen and Dörrscheidt, 1986). Thus, the observed CBV changes in crows support the functional similarity of the Field L complex across different avian species.

The Field L complex, while varying in specific subdivisions and terminology across species, is generally agreed to be organized into three distinct, sandwiched layers: L1, L2, and L3 (Bonke et al., 1979; Fortune and Margoliash, 1992; Vates et al., 1996). L2 serves as the primary recipient of thalamic input from the auditory nucleus ovoidalis (Karten, 1968; Wang et al., 2010). From L2, auditory information is processed and relayed to flanking subregions, L1 and L3. These serve as output layers, sending information to regions such as the nidopallium caudomedial (NCM) and the caudal mesopallium (CM), which are involved in song memory, recognition, and learning (Bailey et al., 2002; Thompson and Gentner, 2010). In oscine birds, including crows, L1 and L3 also project to the dorsal nidopallium near

the song nucleus HVC, particularly to HVC shelf, as well as to the nidopallium caudolaterale, an executive center involved in higher-level processing (Vates et al., 1996; Kersten et al., 2024; Moll et al., 2024). These projections highlight the integrative role of the Field L complex.

In noncorvid songbirds, neurons in the Field L complex show overlapping frequency tuning, which together create an integrated tonotopic representation. Isofrequency contours in the Field L complex run perpendicular to L2 and span all three subfield layers, as demonstrated by earlier electrophysiological studies (Müller and Leppelsack, 1985). In species like European starlings and zebra finches, each of these subfields forms a tonotopic map of the basilar papilla (Capsius and Leppelsack, 1999; Gehr et al., 1999; Nieder and Klump, 1999; 2001). Specifically, the cochleotopic gradient maps lower frequencies to the posterior–dorsal and higher frequencies to the anterior–ventral region of the Field L complex.

Processing hierarchy within the corvid Field L complex

The comparison of CBV changes under different neurophysiological states, along with patterns observed during prolonged sound stimulation, suggests that fUSi can be used to delineate between putative subregions of the Field L complex (Elliott and Theunissen, 2011). Under anesthesia, CBV responses were confined to the central region of Field L, which would correspond to the thalamorecipient input region, L2. The flanking regions, interpreted as L1 and L3, appeared largely inactive during anesthesia. Interestingly, the central region of the Field L complex

exhibited a brief phasic excitation immediately after stimulus onset, followed by pronounced suppression during prolonged sound stimulation. In contrast, flanking regions showed a sustained increase in CBV throughout stimulation.

This is consistent with the electrophysiological properties of neurons in these regions. L2 neurons exhibit the shortest response latencies; neurons in L1 and L3, along with those in the CM and NCM areas, show progressively longer latencies (Calabrese and Woolley, 2015). This pattern supports the notion of a feed-forward processing hierarchy (Wang et al., 2010; Calabrese and Woolley, 2015) that mirrors the principles of information processing seen in the canonical cortical microcircuit, once thought to be exclusive to mammals.

Influence of anesthesia

We observed a significant reduction in stimulus-induced auditory CBV changes under anesthesia compared with the awake state. This aligns with findings from fMRI studies where awake animals exhibit stronger BOLD responses compared with anesthetized ones (Desai et al., 2011; Dinh et al., 2021). Additional evidence comes from human imaging studies (Heinke and Koelschb, 2005) and animal electrophysiological recordings (Gaese and Ostwald, 2001; Syka et al., 2005). In songbirds, both spontaneous and stimulus-induced neuronal activity in the Field L complex are significantly reduced under anesthesia (Capsius and Leppelsack, 1996; Schmidt and Konishi, 1998; Karino et al., 2016).

We used ketamine and xylazine as the primary anesthetic agents. Ketamine functions primarily as an N-methyl-D-aspartate receptor (NMDAR) antagonist, blocking excitatory glutamatergic synaptic transmission (Zanos et al., 2018). The most straightforward interpretation of our findings is that the substantial reduction in stimulus-induced CBV observed in crows under anesthesia reflects reduced neuronal activity. However, we cannot entirely dismiss the possibility that CBV reduction is influenced by direct effects of anesthesia on blood flow via mechanisms affecting the vasculature. Regardless of the exact underlying mechanism, anesthesia clearly leads to a significant underestimation of functional auditory activation. Despite this anesthesia-induced underestimation, the tonotopic mapping is preserved as shown by the across-neurophysiological state MVPA classifier performances.

Effects of stimulus duration

We analyzed a critical parameter for behavioral and physiological studies—the effects of stimulus duration—on CBV responses. CBV changes can be reliably detected with shorter stimuli of 0.5 and 1 s lengths, even at the single-voxel level. Following stimulus onset, CBV signals show a quickly decaying transient increase. Longer stimuli (i.e., 5 s) produce more variable responses (e.g., sustained activity, onset-specific responses, negative deflections). Negative responses have been reported in other studies (olfactory, Boido et al., 2019; visual, Macé et al., 2018; auditory, Rau et al., 2018) and could result from factors like a decrease in neuronal activity leading to decreased blood volume, artery constriction, steal effects, or drainage. It is worth mentioning that widely used methods to identify significantly active voxels by correlating CBV signals with a convolved stimulus vector may miss such complex stimulus-evoked activity.

Amplitudes of initial responses were similar across stimuli durations, indicating robust signal-to-noise ratios. Similarly, studies in macaques have reported comparable response profiles in V1 activity for 0.5 and 1.0 s stimuli (Blaize et al., 2020).

However, differences emerged after the first few seconds when longer stimuli were presented. In rats, barrel CBV responses rapidly return to the baseline after short stimuli but have a prolonged decay beyond stimulus duration for long stimuli (Urban et al., 2015). In behavioral tasks, shorter stimuli are often sufficient to capture relevant activity, even allowing online decoding of eye movement direction during memory-guided saccade tasks (Norman et al., 2021, Griggs et al., 2024).

References

Arya P, Petkova SP, Kulkarni PP, Kolodny NH, Gobes SM (2023) Tracing development of song memory with fMRI in zebra finches after a second tutoring experience. Commun Biol 6:345.

Aydin AK, Haselden WD, Goulam Houssen Y, Pouzat C, Rungta RL, Demené C, Tanter M, Drew PJ, Charpak S, Boido D (2020) Transfer functions linking neural calcium to single voxel functional ultrasound signal. Nat Commun 11:2954.

Bailey DJ, Rosebush JC, Wade J (2002) The hippocampus and caudomedial neostriatum show selective responsiveness to conspecific song in the female zebra finch. J Neurobiol 52:43–51.

Behroozi M, et al. (2020) Event-related functional MRI of awake behaving pigeons at 7T. Nat Commun 11:4715.

Behroozi M, Lorenzi E, Tabrik S, Tegenthoff M, Gozzi A, Güntürkün O, Vallortigara G (2024) Functional MRI of imprinting memory in awake newborn domestic chicks. Commun Biol 7:1326.

Bertolo A, et al. (2021) Whole-brain 3D activation and functional connectivity mapping in mice using transcranial functional ultrasound imaging. J Vis Exp e62267.

Bimbard C, Demene C, Girard C, Radtke-Schuller S, Shamma S, Tanter M, Boubenec Y (2018) Multi-scale mapping along the auditory hierarchy using high-resolution functional ultrasound in the awake ferret. Elife 7: e35028.

Blaize K, et al. (2020) Functional ultrasound imaging of deep visual cortex in awake nonhuman primates. Proc Natl Acad Sci USA 117:14453–14463.

Bluff LA, Kacelnik A, Rutz C (2010) Vocal culture in new caledonian crows Corvus moneduloides. Biol J Linn Soc 101:767–776.

Boido D, et al. (2019) Mesoscopic and microscopic imaging of sensory responses in the same animal. Nat Commun 10:1110.

Bonke BA, Bonke D, Scheich H (1979) Connectivity of the auditory forebrain nuclei in the Guinea fowl Numida meleagris. Cell Tissue Res 200:101–122.

Brecht KF, Hage SR, Gavrilov N, Nieder A (2019) Volitional control of vocalizations in corvid songbirds. PLoS Biol 17:e3000375.

Brecht KF, Westendorff S, Nieder A (2023) Neural correlates of cognitively controlled vocalizations in a corvid songbird. Cell Rep 42:112113.

Brown ED (1985) The role of song and vocal imitation among common crows (Corvus brachyrhynchos). Zeitschrift für Tierpsychologie 68:115–136.

Brunner C, et al. (2020) A platform for brain-wide volumetric functional ultrasound imaging and analysis of circuit dynamics in awake mice. Neuron 108:861–875.

Buxton RB, Uludağ K, Dubowitz DJ, Liu TT (2004) Modeling the hemodynamic response to brain activation. Neuroimage 23:S220–S233.

Calabrese A, Woolley SM (2015) Coding principles of the canonical cortical microcircuit in the avian brain. Proc Natl Acad Sci USA 112:3517–3522.

Capsius B, Leppelsack HJ (1996) Influence of urethane anesthesia on neural processing in the auditory cortex analogue of a songbird. Hear Res 96: 59–70.

Capsius B, Leppelsack H (1999) Response patterns and their relationship to frequency analysis in auditory forebrain centers of a songbird. Hear Res 136:91–99.

Claron J, et al. (2021) Large-scale functional ultrasound imaging of the spinal cord reveals in-depth spatiotemporal responses of spinal nociceptive circuits in both normal and inflammatory states. Pain 162:1047–1059.

Claron J, Provansal M, Salardaine Q, Tissier P, Dizeux A, Deffieux T, Picaud S, Tanter M, Arcizet F, Pouget P (2023) Co-variations of cerebral blood volume and single neurons discharge during resting state and visual cognitive tasks in non-human primates. Cell Rep 42:112369.

Coombs C (1960) Observations on the rook Corvus frugilegus in southwest Cornwall. Ibis 102:394–419.

Cunha FC, Griesser M (2021) Who do you trust? Wild birds use social knowledge to avoid being deceived. Sci Adv 7:eaba2862.

Demené C, et al. (2015) Spatiotemporal clutter filtering of ultrafast ultrasound data highly increases Doppler and fUltrasound sensitivity. IEEE Trans Med Imaging 34:2271–2285.

Demene C, et al. (2017) Functional ultrasound imaging of brain activity in human newborns. Sci Transl Med 9:eaah6756.

Desai M, et al. (2011) Mapping brain networks in awake mice using combined optical neural control and fMRI. J Neurophysiol 105:1393–1405.

Di Ianni T, Ewbank SN, Levinstein MR, Azadian MM, Budinich RC, Michaelides M, Airan RD (2024) Sex dependence of opioid-mediated responses to subanesthetic ketamine in rats. Nat Commun 15:893.

Dinh TNA, Jung WB, Shim HJ, Kim SG (2021) Characteristics of fMRI responses to visual stimulation in anesthetized versus awake mice. Neuroimage 226:117542.

Dizeux A, et al. (2019) Functional ultrasound imaging of the brain reveals propagation of task-related brain activity in behaving primates. Nat Commun 10:1400.

Dooling RJ, Lohr B, Dent ML (2000) Hearing in birds and reptiles. In: Comparative hearing: birds and reptiles. Springer handbook of auditory research (Dooling RJ, Fay RR, Popper AN, eds), vol 13, pp 308–359. New York, NY: Springer.

Edelman BJ, Ielacqua GD, Chan RW, Asaad M, Choy M, Lee JH (2021) High-sensitivity detection of optogenetically-induced neural activity with functional ultrasound imaging. Neuroimage 242:118434.

El Hady A, et al. (2024) Chronic brain functional ultrasound imaging in freely moving rodents performing cognitive tasks. J Neurosci Methods 403:110033.

Elliott TM, Theunissen FE (2011) The avian auditory pallium. In: The auditory cortex (Winer J, Schreiner C, eds), pp 429–442. Boston, MA: Springer.

Emery NJ, Clayton NS (2004) The mentality of crows: convergent evolution of intelligence in corvids and apes. Science 306:1903–1907.

Fortune ES, Margoliash D (1992) Cytoarchitectonic organization and morphology of cells of the field L complex in male zebra finches (Taeniopygia guttata). J Comp Neurol 325:388–404.

Friston KJ, Jezzard P, Turner R (1994) Analysis of functional MRI time-series. Hum Brain Mapp 1:153–171.

Friston KJ, Holmes AP, Poline JB, Grasby PJ, Williams SCR, Frackowiak RS, Turner R (1995) Analysis of fMRI time-series revisited. Neuroimage 2:45–53.

Gaese BH, Ostwald J (2001) Anesthesia changes frequency tuning of neurons in the rat primary auditory cortex. J Neurophysiol 86:1062–1066.

Gehr DD, Capsius B, Gräbner P, Gahr M, Leppelsack HJ (1999) Functional organisation of the field-L-complex of adult male zebra finches. Neuroreport 10:375–380.

Gesnik M, Blaize K, Deffieux T, Gennisson JL, Sahel JA, Fink M, Picaud S, Tanter M (2017) 3D functional ultrasound imaging of the cerebral visual system in rodents. Neuroimage 149:267–274.

Griggs WS, et al. (2024) Decoding motor plans using a closed-loop ultrasonic brain–machine interface. Nat Neurosci 27:196–207.

Heinke W, Koelsch S (2005) The effects of anesthetics on brain activity and cognitive function. Curr Opin Anaesthesiol 18:625–631.

Hoffmann A, Rüttler V, Nieder A (2011) Ontogeny of object permanence and object tracking in the carrion crow, Corvus corone. Anim Behav 82:359–367.

Hopp SL, Jablonski P, Brown JL (2001) Recognition of group membership by voice in Mexican jays, Aphelocoma ultramarina. Anim Behav 62:297–303.

Hu W, Zhu S, Briggs F, Doyley MM (2023) Functional ultrasound imaging reveals 3D structure of orientation domains in ferret primary visual cortex. Neuroimage 268:119889.

Imbault M, Chauvet D, Gennisson JL, Capelle L, Tanter M (2017) Intraoperative functional ultrasound imaging of human brain activity. Sci Rep 7:7304.

Jensen KK, Klokker S (2006) Hearing sensitivity and critical ratios of hooded crows (Corvus corone cornix). J Acoust Soc Am 119:1269–1276.

Karino G, George I, Loison L, Heyraud C, De Groof G, Hausberger M, Cousillas H (2016) Anesthesia and brain sensory processing: impact on neuronal responses in a female songbird. Sci Rep 6:39143.

Karten HJ (1968) The ascending auditory pathway in the pigeon Columba livia telencephalic projections of the nucleus ovoidalis thalami mammals. Brain Res 11:134–153.

Kersten Y, Friedrich-Müller B, Nieder A (2021) A histological study of the song system of the carrion crow (Corvus corone). J Comp Neurol 529:2576–2595.

Kersten Y, Friedrich-Müller B, Nieder A (2022) A brain atlas of the carrion crow (Corvus corone). J Comp Neurol 530:3011–3038.

Kersten Y, Moll FW, Erdle S, Nieder A (2024) Input and output connections of the crow nidopallium caudolaterale. eNeuro 11:ENEURO.0098-24.2024.

Kondo N, Izawa E-I, Watanabe S (2010) Perceptual mechanism for vocal individual recognition in jungle crows (Corvus macrorhynchos): contact call signature and discrimination. Behaviour 147:1051–1072.

Lambers H, Segeroth M, Albers F, Wachsmuth L, van Alst TM, Faber C (2020) A cortical rat hemodynamic response function for improved detection of BOLD activation under common experimental conditions. Neuroimage 208:116446.

Liao DA, Brecht KF, Veit L, Nieder A (2024) Crows 'count' the number of self-generated vocalizations. Science 384:874–877.

Liao DA, Moll FW, Nieder A (2025) Bridging the fields of cognition and birdsong with corvids. Curr Opin Neurobiol 90:102965.

Macé E, Montaldo G, Cohen I, Baulac M, Fink M, Tanter M (2011) Functional ultrasound imaging of the brain. Nat Methods 8:662–664.

Macé É, Montaldo G, Trenholm S, Cowan C, Brignall A, Urban A, Roska B (2018) Whole-brain functional ultrasound imaging reveals brain modules for visuomotor integration. Neuron 100:1241–1251.

Martin K, Cornero FM, Clayton NS, Adam O, Obin N, Dufour V (2024) Vocal complexity in a socially complex corvid: gradation, diversity and lack of common call repertoire in male rooks. R Soc Open Sci 11:231713.

Mates EA, Tarter RR, Ha JC, Clark AB, McGowan KJ (2015) Acoustic profiling in a complexly social species, the American crow: caws encode information on caller sex, identity and behavioural context. Bioacoustics 24:63–80.

Moll FW, Kersten Y, Erdle S, Nieder A (2024) Exploring Anatomical Links Between the Crow's Nidopallium Caudolaterale and its Song System. bioRxiv, 2024-07.

Mooney R (2009) Neural mechanisms for learned birdsong. Learn Mem 16:655–669.

Müller CM, Leppelsack HJ (1985) Feature extraction and tonotopic organization in the avian auditory forebrain. Exp Brain Res 59:587–599.

Nieder A (2023) Neuroscience of cognitive control in crows. Trends Neurosci 46:783–785.

Nieder A, Klump GM (1999) Adjustable frequency selectivity of auditory forebrain neurons recorded in a freely moving songbird via radiotelemetry. Hear Res 127:41–54.

Nieder A, Klump GM (2001) Signal detection in amplitude-modulated maskers. II. Processing in the songbird's auditory forebrain. Eur J Neurosci 13:1033–1044.

Norman KA, Polyn SM, Detre GJ, Haxby JV (2006) Beyond mind-reading: multi-voxel pattern analysis of fMRI data. Trends Cogn Sci (Regul Ed) 10:424–430.

Norman SL, et al. (2021) Single-trial decoding of movement intentions using functional ultrasound neuroimaging. Neuron 109:1554–1566.

Nunez-Elizalde AO, Krumin M, Reddy CB, Montaldo G, Urban A, Harris KD, Carandini M (2022) Neural correlates of blood flow measured by ultrasound. Neuron 110:1631–1640.

Pnevmatikakis EA, Giovannucci A (2017) NoRMCorre: an online algorithm for piecewise rigid motion correction of calcium imaging data. J Neurosci Methods 291:83–94.

Rabut C, Correia M, Finel V, Pezet S, Pernot M, Deffieux T, Tanter M (2019) 4D functional ultrasound imaging of whole-brain activity in rodents. Nat Methods 16:994–997.

Rabut C, Norman SL, Griggs WS, Russin JJ, Jann K, Christopoulos V, Liu C, Andersen AR, Shapiro GM (2024) Functional ultrasound imaging of human brain activity through an acoustically transparent cranial window. Sci Transl Med 16:eadj3143.

Rau R, Kruizinga P, Mastik F, Belau M, de Jong N, Bosch JG, Scheffer W, Maret G (2018) 3D functional ultrasound imaging of pigeons. Neuroimage 183:469–477.

Rübsamen R, Dörrscheidt G (1986) Tonotopic organization of the auditory forebrain in a songbird, the European starling. J Comp Physiol A 158:639–646.

Schmidt MF, Konishi M (1998) Gating of auditory responses in the vocal control system of awake songbirds. Nat Neurosci 1:513–518.

Siegenthaler D, et al. (2024) Visual objects refine head direction coding. bioRxiv, 2024-10.

Sieu LA, Bergel A, Tiran E, Deffieux T, Pernot M, Gennisson JL, Tanter M, Cohen I (2015) EEG and functional ultrasound imaging in mobile rats. Nat Methods 12:831–834.

Syka J, Kuta D, Popelár J (2005) Responses to species-specific vocalizations in the auditory cortex of awake and anesthetized Guinea pigs. Hear Res 206: 177–184.

Szipl G, Ringler E, Spreafico M, Bugnyar T (2017) Calls during agonistic interactions vary with arousal and raise audience attention in ravens. Front Zool 14:1–13.

Takahashi DY, El Hady A, Zhang YS, Liao DA, Montaldo G, Urban A, Ghazanfar AA (2021) Social-vocal brain networks in a non-human primate. *BioRxiv*, 2021-12.

Taylor AH (2014) Corvid cognition. Wiley interdisciplinary reviews. Cogn Sci 5:361–372.

Thompson JV, Gentner TQ (2010) Song recognition learning and stimulus-specific weakening of neural responses in the avian auditory forebrain. J Neurophysiol 103:1785–1797.

Tiran E, Ferrier J, Deffieux T, Gennisson JL, Pezet S, Lenkei Z, Tanter M (2017) Transcranial functional ultrasound imaging in freely moving awake mice and anesthetized young rats without contrast agent. Ultrasound Med Biol 43:1679–1689.

Ungurean G, Behroozi M, Böger L, Helluy X, Libourel PA, Güntürkün O, Rattenborg NC (2023) Wide-spread brain activation and reduced CSF flow during avian REM sleep. Nat Commun 14:3259.

Urban A, Dussaux C, Martel G, Brunner C, Mace E, Montaldo G (2015) Real-time imaging of brain activity in freely moving rats using functional ultrasound. Nat Methods 12:873–878.

Van Ruijssevelt L, De Groof G, Van der Kant A, Poirier C, Van Audekerke J, Verhoye M, Van der Linden A (2013) Functional magnetic resonance imaging (FMRI) with auditory stimulation in songbirds. J Vis Exp 76: 4369.

Van Ruijssevelt L, Chen Y, von Eugen K, Hamaide J, De Groof G, Verhoye M, Güntürkün O, Woolley SC, Van der Linden A (2018) fMRI reveals a novel region for evaluating acoustic information for mate choice in a female songbird. Curr Biol 28:711–721.e6.

Vates GE, Broome BM, Mello CV, Nottebohm F (1996) Auditory pathways of caudal telencephalon and their relation to the song system of adult male zebra finches. J Comp Neurol 366:613–642.

Wagener L, Nieder A (2020) Categorical auditory working memory in crows. iScience 23:101737.

Wang Y, Brzozowska-Prechtl A, Karten HJ (2010) Laminar and columnar auditory cortex in avian brain. Proc Natl Acad Sci USA 107:12676–12681.

Wascher CA, Szipl G, Boeckle M, Wilkinson A (2012) You sound familiar: carrion crows can differentiate between the calls of known and unknown heterospecifics. Anim Cogn 15:1015–1019.

Woolley SM, Casseday JH (2005) Processing of modulated sounds in the zebra finch auditory midbrain: responses to noise, frequency sweeps, and sinusoidal amplitude modulations. J Neurophysiol 94: 1143–1157.

Zanos P, et al. (2018) Ketamine and ketamine metabolite pharmacology: insights into therapeutic mechanisms. Pharmacol Rev 70:621–660.

Zhang YS, Takahashi DY, El Hady A, Liao DA, Ghazanfar AA (2022) Active neural coordination of motor behaviors with internal states. Proc Natl Acad Sci USA 119:e2201194119.